JACS
JOURNAL OF THE AMERICAN CHEMICAL SOCIETY
Article
Cite This: J. Am. Chem. Soc. 2018, 140, 11076−11084
pubs.acs.org/JACS

Enhanced Stability of the Carba-*closo*-dodecaborate Anion for High-Voltage Battery Electrolytes through Rational Design

Nathan T. Hahn,[†,‡,∥] Trevor J. Seguin,[†,§,∥] Ka-Cheong Lau,[†,⊥] Chen Liao,[†,⊥] Brian J. Ingram,[†,⊥] Kristin A. Persson,[*,†,§,#] and Kevin R. Zavadil[*,†,‡]

[†]Joint Center for Energy Storage Research, Argonne, Illinois 60439, United States
[‡]Material, Physical and Chemical Sciences Center, Sandia National Laboratories, Albuquerque, New Mexico 87158, United States
[§]Energy Technologies Division, Lawrence Berkeley National Laboratory, Berkeley, California 94720, United States
[⊥]Chemical Sciences and Engineering Division, Argonne National Laboratory, Lemont, Illinois 60439, United States
[#]Department of Materials Science, University of California Berkeley, Berkeley, California 94720, United States

Supporting Information

ABSTRACT: Future energy applications rely on our ability to tune liquid intermolecular interactions and achieve designer electrolytes with highly optimized properties. In this work, we demonstrate rational, combined experimental−computational design of a new carba-*closo*-dodecaborate-based salt with enhanced anodic stability for Mg energy storage applications. We first establish, through a careful examination using a range of solvents, the anodic oxidation of a parent anion, the carba-*closo*-dodecaborate anion at 4.6 V vs $Mg^{0/2+}$ (2.0 vs $Fc^{0/+}$), a value lower than that projected for this anion in organic solvent-based electrolytes and lower than weakly associating bis(trifluoromethylsulfonyl)imide and tetrafluoroborate anions. Solvents such as acetonitrile, 3-methylsulfolane, and 1,1,1,3,3,3-hexafluoroisopropanol are shown to enable the direct measurement of carba-*closo*-dodecaborate oxidation, where the resultant neutral radical drives passive film formation on the electrode. Second, we employ computational screening to evaluate the impact of functionalization of the parent anion on its stability and find that replacement of the carbon-vertex proton with a more electronegative fluorine or trifluoromethyl ligand increases the oxidative stability and decreases the contact-ion pair formation energy while maintaining reductive stability. This predicted expansion of the electrochemical window for fluorocarba-*closo*-dodecaborate is experimentally validated. Future work includes evaluation of the viability of these derivative anions as efficient and stable carriers for energy storage as a function of the ionic transport through the resulting surface films formed on candidate cathodes.

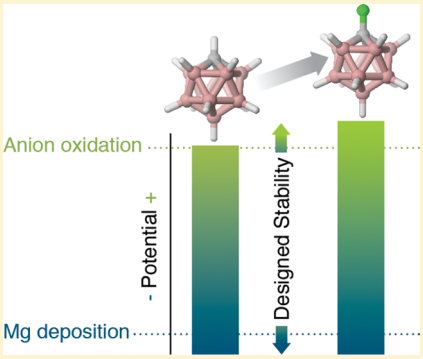

INTRODUCTION

Liquid electrolytes designed with enhanced solubility, ionic transport, and electrochemical stability are essential for enhancing the performance of existing and enabling new electrical energy storage and conversion devices. Success demonstrated in the suppression of ion pairing in Li ion electrolytes using weakly coordinating anions (WCA)[1] to support increased Li^+ solvation and corresponding mobility must be extended to emergent Mg^{2+} ion systems (and other multivalents) where solvation is challenged by the higher charge density and hence electrostatic binding energy of the cation. Various classes of WCAs have shown promise as supporting electrolyte anions for Mg^{2+} including the carba-*closo*-borates,[2] alkoxyborates,[3] and alkoxyaluminates.[4] Each of these anion classes possesses rich substitutional chemistry that can be exploited to correlate anion structure with electrolyte function and stability, thereby enabling rational electrolyte design. The carba-*closo*-dodecaborate anion is of particular interest because of its reported electrochemical stability and solubility in polyether solvents.[2]

A focus on candidate Mg salts is further motivated by the fact that emerging energy storage concepts based on Mg metal anodes and Mg^{2+} intercalation cathodes could potentially exceed the energy storage density of Li-ion batteries, provided functional, high-voltage cathodes and compatible wide electrochemical window electrolytes are concurrently developed.[5,6] To this end, a variety of anions have been explored ranging from chloro complexes,[7−9] which are unstable at potentials for target high-voltage cathodes,[10] to conventional WCAs such as PF_6^-,[11] exhibiting insufficient cathodic stability.[12] Mg salts based on carba-*closo*-borate anions have recently been demonstrated as promising supporting electrolytes in ethers with the potential for expanding the electrochemical stability window.[2,13,14] Magnesium carba-*closo*-dodecaborate ($Mg[HCB_{11}H_{11}]_2$) was explored in triethylene glycol dimethyl ether (triglyme, G3) and tetraethylene glycol dimethyl ether (tetraglyme, G4) and shown to yield a sustainable >99%

Received: June 6, 2018
Published: July 30, 2018

DOI: 10.1021/jacs.8b05967
J. Am. Chem. Soc. 2018, 140, 11076−11084

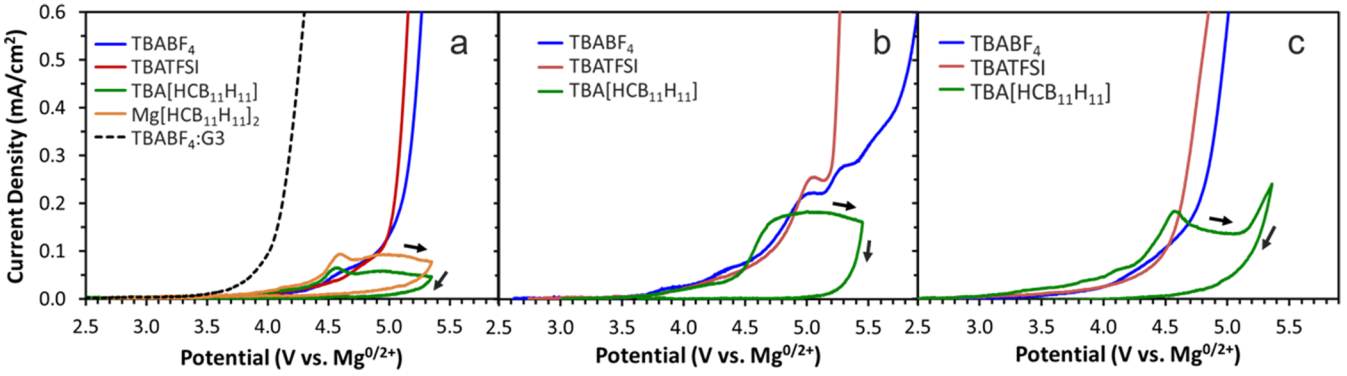

Figure 1. Onset of electrolyte oxidation at Pt in 0.25 M TBABF4, TBATFSI, and $TBACB_{11}H_{11}$ in 3-MeTMS (a), HFIP (b), and MeCN (c). Responses of $Mg(HCB_{11}H_{11})_2$ in 3-MeTMS and $TBABF_4$ in G3 (a) are included to highlight the cation-independent $HCB_{11}H_{11}^-$ response and the stability limit of the reference G3 glyme. Arrows indicate the sweep direction during the $HCB_{11}H_{11}^-$ voltammetry (scan rate = 10 mV/s).

Coulombic efficiency (CE) for Mg cycling in G4 with an oxidation threshold dictated by the glyme solvent employed and the electrode material.[2] Full cell cycling using the G4 version of this electrolyte was reported using the intermediate voltage cathode α-MnO_2 at cell charging potentials up to 3.5 V (vs $Mg^{0/2+}$). Magnesium carba-*closo*-decaborate ($Mg[HCB_9H_9]_2$) has also been explored in G4 and exhibits qualitatively reversible Mg plating and stripping coupled with an oxidation threshold, again dictated by the G4 solvent and the electrode material.[15] In both of these cases, the expected anodic stability gain with the use of the carba-*closo*-borate anion is not realized because the less anodically stable glymes/ethers solvents are selected for cathodic stability (i.e., Mg metal compatibility). The carba-*closo*-borate material class further offers the opportunity to tailor anion stability through systematic changes in cage functionalization and/or size. Whereas a considerable amount of electrochemical stability characterization has been conducted on carba-*closo*-borates, virtually no data has been reported using solvents and salt concentrations relevant to a practical secondary battery.[16−18] Furthermore, to our knowledge, the long-held consensus that the unfunctionalized $HCB_{11}H_{11}^-$ anion is "weakly coordinating" has never been subject to scrutiny by investigation such as quantification of ion-association strength by first-principles calculations. In the interest of continued development of carba-*closo*-borate-based multivalent electrolytes toward improved secondary energy storage, further theoretical exploration of the vast space of chemical derivatizations and corresponding effects on electrolyte properties is warranted. Therefore, our goal is to understand how the structure of carba-*closo*-borate anions determines their stability and extent of ion association as electrolyte constituents.

In this paper, we employ a combined experimental−theoretical synergistic approach of first-principles calculations, synthesis, and electrochemical characterization to (i) determine the limit of the electrochemical stability of $HCB_{11}H_{11}^-$ relative to other key anions used for energy storage and in solvents with extended anodic windows and (ii) design novel $HCB_{11}H_{11}^-$ derivatives which combine improved anodic stability with Mg anode compatibility. Electrochemical measurements in oxidatively stable solvents, including acetonitrile (MeCN), 3-methylsulfolane (3-MeTMS), and 1,1,1,3,3,3-hexafluoroisopropanol (HFIP), show that $HCB_{11}H_{11}^-$ is less anodically stable than the traditional energy storage anions bis(trifluoromethylsulfonyl)imide ($TFSI^-$) and tetrafluoroborate (BF_4^-) and are validated through quantum chemical calculation of oxidation potentials. These experiments further demonstrate that oxidation of the $HCB_{11}H_{11}^-$ anion to the expected unstable neutral $HCB_{11}H_{11}^{\bullet}$ radical leads to electrode passivation behavior, which does not occur in electrolytes containing the traditional anions. A broad computational screening of 28 possible $HCB_{11}H_{11}^-$ derivatives identifies several promising candidates for improved electrochemical stability, specifically those containing electron-withdrawing substituents at the C-vertex site. On the basis of these screening results, synthesis and electrochemical characterization of the computationally predicted monofluoro ($FCB_{11}H_{11}^-$) as well as the monotrifluoromethyl ($CF_3CB_{11}H_{11}^-$) derivatives are discussed. $RCB_{11}H_{11}^-$ anions (R = any moiety bonded to the vertex carbon, including H) derived using simple carbon vertex substitution are shown to offer a path forward to creating an efficient high-voltage Mg battery electrolyte.

RESULTS AND DISCUSSION

The oxidation potential of the original $HCB_{11}H_{11}^-$ anion is first established by utilizing noncoordinating cations and a variety of thoroughly dried solvents with high anodic stability. A previous study indicated that glymes such as G3 or G4 impose an anodic stability limit that prevents characterization of $HCB_{11}H_{11}^-$ oxidation.[2] Therefore, solvents were selected based on a computed oxidation potential greater than that of G3 at 5.32 V, identifying 3-MeTMS (5.75 V), HFIP (7.10 V), and MeCN (7.42 V) as candidates. The voltammetric responses of these three solvents using 0.25 M $TBABF_4$ (BF_4^- E_{ox} = 7.47 V) as a supporting electrolyte are shown in Figure 1a−c. Responses show the background current density deviates from the capacitive charging values of 4 $\mu A/cm^2$ at 3.7 V (vs $Mg^{0/2+}$), gradually increasing until a more definite electrolyte breakdown onset is observed at 4.7, 5.0, and 5.6 V for MeCN, 3-MeTMS, and HFIP, respectively. The observed lower than computed stability of MeCN is consistent with previous reports of an anodic threshold ranging from 5.0 to 5.3 V vs $Mg^{0/2+}$ (from 2.6 to 2.9 V vs $Ag^{0/+}$ [10 mM]), commonly defined as the potential required to generate 1 mA/cm^2 at Pt and whose value is dependent on the supporting electrolyte salt used.[19−21] The origin of this decreased stability has been ascribed to anion-initiated oxidation of MeCN, arguing that the anion−solvent complex dictates the stability of the electrolyte, a concept for which computational and experimental correlations are reported for lithium salts in aprotic solvents.[22,23] The characteristic shape and magnitude of the

DOI: 10.1021/jacs.8b05967
J. Am. Chem. Soc. 2018, 140, 11076−11084

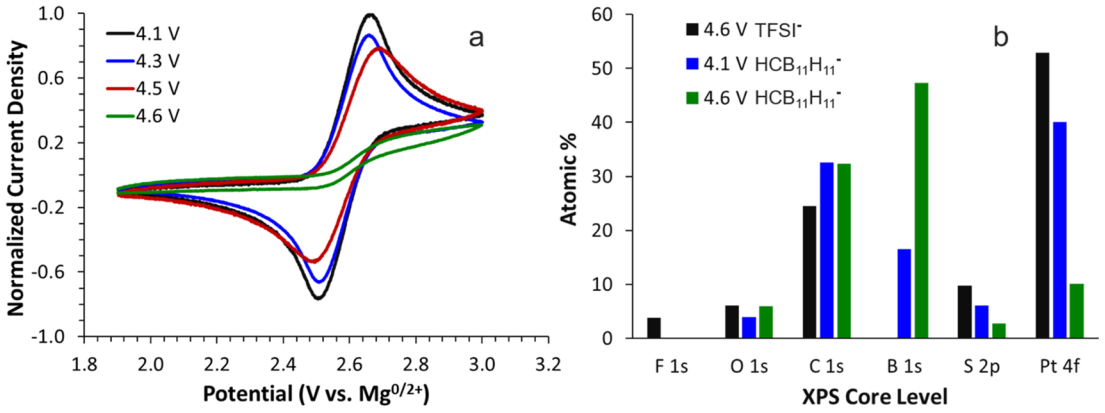

Figure 2. (a) CV response of Fc before and after polarization of the Pt electrode up to 4.6 V in $HCB_{11}H_{11}^-$ solutions in 3-MeTMS. Currents displayed for separate experiments are normalized to the peak oxidative current measured in their respective initial electrode states. (b) Results of XPS quantification of surface species present on electrodes polarized in the presence or absence of $HCB_{11}H_{11}^-$.

initial gradual increase in current for HFIP appears dependent upon native solvent impurities and is consistent with published voltammetric data for the HFIP solvent.[18,24] Variation in impurity response and anion−solvent coupling aside, the voltammetric data confirm solvent−anodic stabilities for MeCN, 3-MeTMS, and HFIP that are greater than those of the representative polyether G3, which oxidizes at approximately 4.0 V (Figure 1a), providing an opportunity to establish more definitively the occurrence and consequence of $HCB_{11}H_{11}^-$ oxidation, which has not previously been reported. The anodic stability thresholds of other polyether solvents (DME and G4) fall within a similar range to G3, between 4.0 and 4.2 V (Supporting Information, Figure S1).

Introduction of $HCB_{11}H_{11}^-$ by way of TBA[$HCB_{11}H_{11}$] or Mg[$HCB_{11}H_{11}$]$_2$ into a 3-MeTMS-, MeCN-, or HFIP-based electrolyte yields a distinctive change in the current−potential response. In all solvents an increase in current density is measured at potentials between 4.4 and 4.6 V, followed by suppression of further electrolyte breakdown and the absence of significant cathodic current density on the reverse potential sweep. In 3-MeTMS and MeCN, the TBA[$HCB_{11}H_{11}$] and Mg[$HCB_{11}H_{11}$]$_2$ salts exhibit a discrete current peak at ca. 4.6 V, followed by a current density plateau, while responses in HFIP yield a single broad current density plateau beginning at 4.6 V. This general behavior is consistent across a range of cations and electrode materials (Supporting Information, Figure S2) and therefore must be driven by the anion. The consistent current onsets and masking of additional anodic current increases from solvent and/or impurity oxidation above 4.6 V, in stark contrast to both $TFSI^-$- and BF_4^--based salts, indicates that the $HCB_{11}H_{11}^-$ anion is oxidized at this potential to the neutral radical $HCB_{11}H_{11}^{\bullet}$, which subsequently reacts at the electrode surface leading to the onset of a passivating surface film.

The formation of this transient $HCB_{11}H_{11}^{\bullet}$ radical is expected based on previous studies which have demonstrated that oxidation of various methyl-substituted carba-*closo*-dodecaborate anions produces a stable and electrochemically reducible radical species.[18] The neutral radical of the unsubstituted $HCB_{11}H_{11}^-$ anion, however, is regarded as unstable and therefore susceptible to rapid decay through reaction with other electrolyte constituents, including $HCB_{11}H_{11}^-$ itself.[18] Such reactions apparently passivate the electrode toward bulk electrolysis of the electrolyte to varying degrees with 3-MeTMS and HFIP showing more extensive passivation and decreased current density up to 5.4 V and MeCN exhibiting transpassive behavior with a current density increase at 5.2 V. Passivation is more clearly demonstrated by comparing pre- and postcycle response of the electrode toward ferrocene, as shown in Figure 2a. In this experiment, the electrode is swept to and held at a potential prior to or at peak oxidation for 600 s and then transferred back to the ferrocene-containing electrolyte. Ferrocene oxidation and subsequent ferrocenium cation reduction are impeded as a passive film begins to form at 4.3 V and fully forms at 4.6 V, blocking access of ferrocene. Electrodes either polarized to lower potentials (e.g., 4.1 V) in the presence of $HCB_{11}H_{11}^-$ or polarized to 4.6 V in the presence of other anions (e.g., BF_4^-, $TFSI^-$) did not exhibit this passivation response for any of these solvents. On the basis of the results of these control experiments, we can attribute the general anodic passivation response to the presence of the $HCB_{11}H_{11}^-$ anion, independent of other constituents. Surface analysis conducted with XPS following polarization of electrodes to 4.6 V reveals that $HCB_{11}H_{11}^-$-derived species constitute the primary film components (Figure 2b). The formation of a uniform film of several nanometers thickness at 4.6 V in the presence of $HCB_{11}H_{11}^-$ is evident through the attenuation of Pt(4f) photoelectron yield, while the prevalence of $HCB_{11}H_{11}^-$ species within the film is argued through the corresponding enhancement of B(1s) photoelectron yield. ToF-SIMS analysis confirms the presence of the parent anion within the film along with higher molecular weight species whose isotopic patterns indicate the formation of a modified boron cage (Supporting Information, Figure S3). Passivation due to $HCB_{11}H_{11}^-$ oxidation has not been previously reported, and its observation in this case is enabled using relevant salt concentrations, sufficiently stable solvents such as 3-MeTMS, HFIP, and MeCN, and potentiostatic hold experiments.

Our results demonstrate that the $HCB_{11}H_{11}^-$ anion undergoes electrooxidation at a potential of 4.6 V vs $Mg^{0/2+}$ or 2.0 V vs $Fc^{0/+}$ in 3-MeTMS, HFIP, and MeCN (24 °C), establishing a benchmark stability for $HCB_{11}H_{11}^-$ in organic solvents. This value agrees with the most recently published data for Cs[$HCB_{11}H_{11}$] measured in HFIP (23 °C).[18] In MeCN, the absence of a detectable $HCB_{11}H_{11}^-$ oxidation signature in previous reports lead to claims of stability greater than that of MeCN at 2.05 V vs $Fc^{0/+}$.[2,13,16,17] A likely

DOI: 10.1021/jacs.8b05967
J. Am. Chem. Soc. 2018, 140, 11076−11084

explanation for the absence of signature in a mixed supporting electrolyte ($HCB_{11}H_{11}^-$ and BF_4^-) is the masking of the $HCB_{11}H_{11}^-$ response by electrolyte decomposition given the proximity of anion and solvent oxidation thresholds. Measurements made duplicating previously employed low $HCB_{11}H_{11}^-$ concentration, added secondary supporting electrolyte, and high sweep rate conditions[16−18] lack the passivation response that serves to help differentiate between superimposed $HCB_{11}H_{11}^-$ and secondary salt−solvent oxidation (Supporting Information, Figure S4). Alternately, the lack of an observable $HCB_{11}H_{11}^-$ oxidation signature reported for moderate Mg-$[HCB_{11}H_{11}]_2$ concentration (0.15 M in MeCN) at an extremely slow sweep rate (0.05 mV/s) likely results from complete formation of the passivating surface film at a greatly reduced current, followed by film breakdown and MeCN oxidation at potentials greater than the onset potential measured in the absence of $HCB_{11}H_{11}^-$ (Supporting Information, Figure S5).[2] A report of enhanced anodic stability of phenylmagnesium carba-*closo*-dodecaborate (PhMg-$[HCB_{11}H_{11}]^\bullet$) appears to be governed by the reaction of the phenyl radical at Pt inhibiting both solvent (1,2-dimethoxyethane) and $HCB_{11}H_{11}^-$ oxidation.[13,19] Our results clearly establish the oxidation of the $HCB_{11}H_{11}^-$ anion at lower than previously projected potentials.

This benchmark value of stability places $HCB_{11}H_{11}^-$ as the least stable within the anion series explored (Figure 1a) according to the trend $HCB_{11}H_{11}^-$ (4.6 V) < $TFSI^-$ (4.9 V) < BF_4^- (above 5.0 V). Comparison of the theoretical oxidation potential computed for $HCB_{11}H_{11}^-$, $TFSI^-$, and BF_4^- in this work yields a trend of $HCB_{11}H_{11}^-$ (4.89 V) < $TFSI^-$ (5.05 V) < BF_4^- (7.47 V) that is qualitatively consistent with the experimental data. Quantitative differences, most notably for BF_4^-, arise because the computational method employed does not explicitly account for the solvated state of the anion. The experimental data presented herein demonstrate that the stability of the electrolyte is determined by the $HCB_{11}H_{11}^-$ anion, being consistent across three solvents, three cations, and two electrode types. Solvent-specific computation shows only a 50 mV variation in E_{ox} of $HCB_{11}H_{11}^-$when MeCN, HFIP, and 3-MeTMS are implicitly treated (5.2 V average) and 100 mV with one explicit solvent molecule included (5.3 V average), further confirming the anion's role. Despite the driving role of the anion, the solvent does participate in subsequent passive film formation as MeCN, a demonstrated electronically conductive surface film former,[25] exhibits both an earlier onset of transpassive behavior and the presence of $HCB_{11}H_{(11-x)}CN_x$ adducts within the film (Supporting Information, Figure S3). The present data identifies a lower than previously projected oxidative stability for $HCB_{11}H_{11}^-$, raising the question of whether synthetic modification of this anion could be used to improve oxidative stability while maintaining reductive stability to facilitate high-voltage Mg battery operation.

To explore possible improvements in the anodic stability of $HCB_{11}H_{11}^-$ we employed a high-throughput computational screening methodology to select optimal derivatives. Theoretical calculations based on first-principles and classical mechanics have proved indispensable toward prediction and analysis of electrolyte properties such as electrochemical stability, diffusion, solubility, conductivity, and viscosity.[26−30] However, this method of investigation has yet to be applied toward some of the promising multivalent ion secondary battery electrolytes discovered in more recent years, such as those containing carba-*closo*-borate anions. Balancing anticipated ease of anion synthesis with its predicted oxidative stability (at a cathode) and reductive stability (at a Mg anode) leads to the hypothesis that a single substitution of the $HCB_{11}H_{11}^-$ cage could afford a realizable improvement in its properties. Furthermore, selective derivatization of B sites on the $HCB_{11}H_{11}^-$ cage has been demonstrated to significantly increase the oxidative stability of the anion, although at the cost of decreased reductive stability in every case.[17,18] In this work, the basic $HCB_{11}H_{11}^-$ framework was screened using 28 potential functional groups at the C site (see Figure 3) by

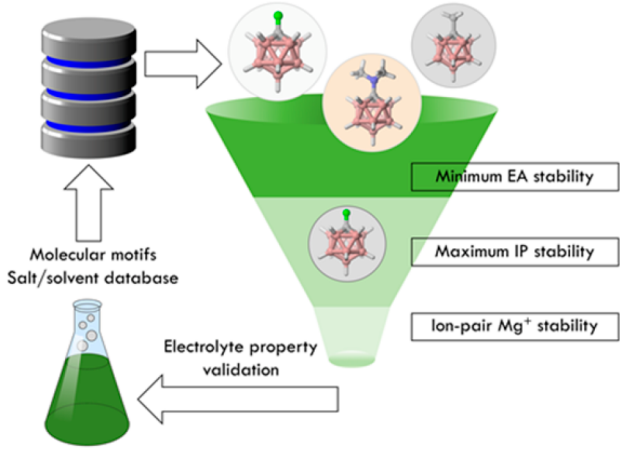

Figure 3. Coupled computational screening and experimental validation was used to identify electrochemically stable $RCB_{11}H_{11}^-$ anion derivatives.

calculating the resulting adiabatic electron affinity (EA) and ionization potential (IP) after functionalization and converting these to reduction and oxidation potentials with respect to the Mg/Mg^{2+} potential (see Computational Methods).

The anodic stability of the various derived salts is clearly dependent on the electronic effect of the C substituent. We find greater stability associated with electron-withdrawing groups (e.g., CF_3, F, and NO_2) and lower stability associated with electron-donating groups (e.g., alkyl, alkoxy, and amino), examples of which are displayed in Figure 4a. The variation of anodic stability with respect to the electronic effect of the substituent is likely due to the corresponding modulation of electron density in the cage. The cathodic stability, however, showed no clear trend with respect to the nature of the substituent. Select derivatives, found in computations to have the raised anodic stability compared to the parent anion, exhibited spontaneous, irreversible decomposition when attempting to optimize the dianion structure to determine cathodic stability under the adiabatic approximation. For example, the $(CF_2)_4CF_5$ and C_6F_5 groups were found to be prone to decomposition by dissociation of a fluorine atom upon reduction, though most groups withstood both oxidation and reduction without any sort of decomposition. A complete list of the 28 C-functionalized $RCB_{11}H_{11}^-$ anions evaluated by first-principles calculations are provided in the Supporting Information, Table S1.

Synthesis and voltammetry of the fluoro-carba-*closo*-dodecaborate anion ($FCB_{11}H_{11}^-$) were conducted to validate these computational results. The computed change in the oxidation potential with substitution of the H−C hydrogen by strong electron-withdrawing groups such as F or CF_3 indicate

DOI: 10.1021/jacs.8b05967
J. Am. Chem. Soc. 2018, 140, 11076−11084

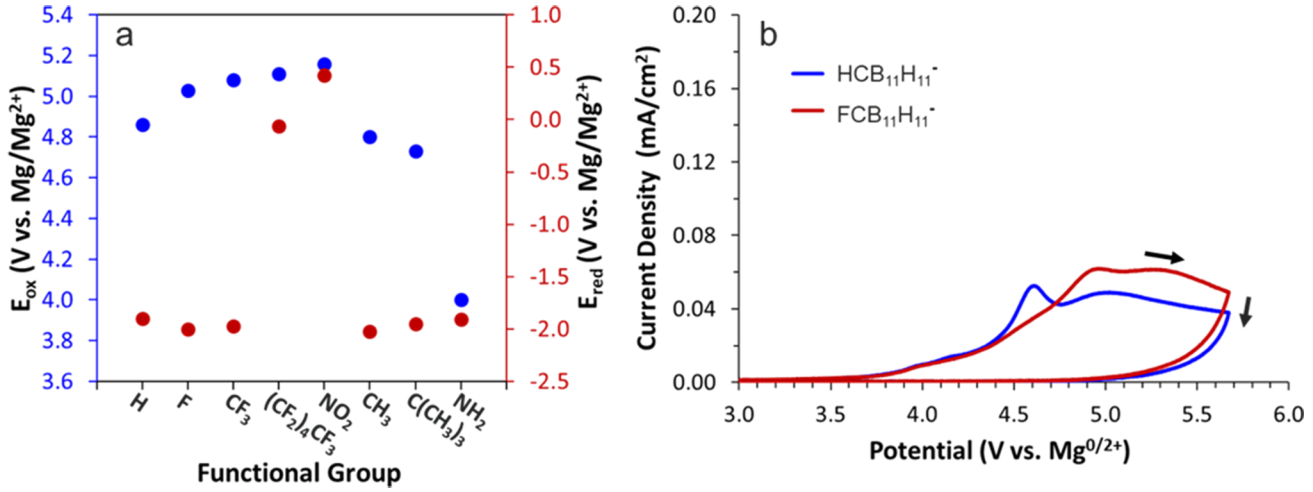

Figure 4. (a) First-principles calculations of R-$CB_{11}H_{11}^-$ E_{ox} and E_{red} as a function of substituent at the carbon. (b) Voltammetric comparison of TBA[$HCB_{11}H_{11}$] and TBA[$FCB_{11}H_{11}$] anodic behavior at 150 mM in 3-MeTMS (scan rate = 10 mV/s).

an ~200 mV increase in E_{ox} accompanied by no significant change in E_{red} (~10 mV decrease, see Figure 4a). Voltammetry of the TBA salt of $FCB_{11}H_{11}^-$ is compared with that of $HCB_{11}H_{11}^-$ in 3-MeTMS, as seen in Figure 4b. Results show that these two anions exhibit qualitatively similar anodic behavior, with the C-fluorinated derivative yielding an oxidation wave that is shifted by approximately +300 mV to 4.9 V. This shift is consistent with the $FCB_{11}H_{11}^-$ anion's predicted higher oxidation potential, thereby validating the computational trend of enhanced anodic stability with fluorination of the carbon. A similar extent of passivation is observed with $FCB_{11}H_{11}^-$ as for $HCB_{11}H_{11}^-$, arguing that the reactivity of the radical is not significantly impacted by functionalization. This observation is consistent with a previous report arguing that halogenation of the boron vertices of $HCB_{11}H_{11}^-$ does not confer additional stability to the neutral radical analog.[18] A measurement of the anodic stability of the CF_3 derivative was not possible as yet due to a low yield from the reported synthesis and purification.[31] Several trifluoromethylation protocols were attempted to access the CF_3 derivative in higher yield, but these methods failed to afford the desired product owing to the chemical inertness of the $HCB_{11}H_{11}^-$ cage.[32−35] The synthesis and electrochemical measurements of the CF_3 derivative will be the subject of future investigations. The similar yet shifted electrochemical responses for $HCB_{11}H_{11}^-$ and $FCB_{11}H_{11}^-$ further demonstrate that $RCB_{11}H_{11}^-$ oxidation gives rise to the anodic signature and that these anions are responsible for passive film formation.

In addition to intrinsic anion stability, understanding the ionic association characteristics of $Mg[RCB_{11}H_{11}]_2$ salts is also critical as association dictates ionic transport properties and the stability of the anion under Mg plating conditions. Recently, Rajput et al. identified the critical coupling between the presence of contact ion pairs and the stability of the salt anion.[30] Specifically, at metal potentials, the ion pair undergoes a transient, partial reduction at the Mg cation center ($Mg^{2+} \rightarrow Mg^+$), which activates the anion to render it susceptible to decomposition, thereby limiting the cathodic stability of the electrolyte.[30,36] Such a mechanism appears to operate in the $MgTFSI_2$/glyme electrolyte system. Hence, the specifics of contact ion pairing—its strength and coordination—are of vital importance to the stability of a proposed salt anion during Mg plating, and such an understanding is required within the $RCB_{11}H_{11}^-$ design space. Sampling the possible coordination sites in the $Mg^{2+}/HCB_{11}H_{11}^-$ ion pair indicates that the lowest energy configuration is where the Mg cation is bound to a triangular set of borons consisting of the boron antipodal to the carbon and two of the adjacent lower belt borons (Figure 5a). Similar binding has been seen with other metals, for

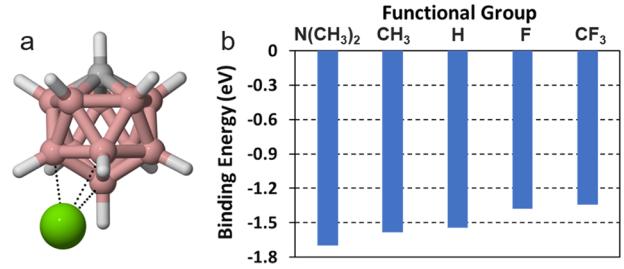

Figure 5. (a) Preferred (tridentate) coordination in $Mg^{2+}/RCB_{11}H_{11}^-$ ion pairs. (b) Cation/anion binding energy (eV) for selected $Mg^{2+}/RCB_{11}H_{11}^-$ ion pairs.

example in the $Cp^*Zr(CH_3)_2(HCB_{11}H_{11})$ complex.[37] This binding is due to the polarization of $HCB_{11}H_{11}^-$ such that the half of the cage opposite the carbon apex bears the most negative electrostatic potential (ESP).

The preferred coordination site of Mg^{2+} is maintained across several of the $HCB_{11}H_{11}^-$ derivatives considered in this study, and weaker and stronger binding energies are associated with electron-withdrawing (fluoro and trifluoromethyl) and electron-donating (alkyl and amino) groups, respectively (Figure 5b). The ESP shows that the variation in binding strength arises from the corresponding modulation of electron density at the coordination site. For example, in Figure 6, the ESP in the plane of Mg^{2+}, the boron antipodal to carbon, and the midpoint of the two adjacent borons bound to Mg^{2+} shows withdrawal of electron density from the coordination site in $FCB_{11}H_{11}^-$ vs $HCB_{11}H_{11}^-$.

The extent of ionic association for electrolytes can be predicted in part from the cation−anion binding strength. The present data show that $FCB_{11}H_{11}^-$ is more weakly coordinating than the parent $HCB_{11}H_{11}^-$ anion, indicating potential for improvement in conductivity and charge transfer in secondary

DOI: 10.1021/jacs.8b05967
J. Am. Chem. Soc. 2018, 140, 11076−11084

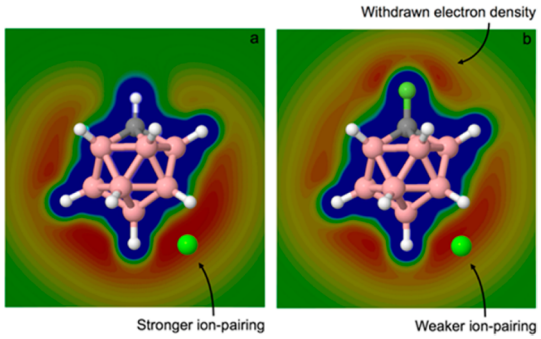

Figure 6. Electrostatic potential imposed by the anion in the plane of Mg^{2+}, the boron antipodal to carbon, and the midpoint of the two adjacent borons bound to Mg^{2+} for the (a) $Mg^{2+}/HCB_{11}H_{11}^-$ and (b) $Mg^{2+}/FCB_{11}H_{11}^-$ ion pairs. Red = −4.4 eV; Blue = 0.0 eV.

battery applications. A similar decrease in binding strength between the two anions is shown when modeling a triglyme solvent molecule bound to Mg^{2+} explicitly to fill the hexacoordinate binding environment typically seen of the Mg^{2+} cation (Supporting Information, Figure S6). This prediction of enhanced transport is confirmed at low carborate concentration in G3 (60 mM) where we measure an approximate 40% increase in conductivity for $FCB_{11}H_{11}^-$ relative to $HCB_{11}H_{11}^-$ (0.14 vs 0.1 mS·cm^{-1} at 25 °C).

To validate the expected cathodic stability of the parent $HCB_{11}H_{11}^-$ and $FCB_{11}H_{11}^-$ derivative under Mg deposition conditions, bond dissociation energies were computed for $RCB_{11}H_{11}^-$ anions coordinated to either a Mg^{2+} cation (i.e., before electron transfer) or a Mg^+ cation (i.e., after initial electron transfer). Bond dissociation energies were first determined for the C−R bond and each unique B−H bond in the $RCB_{11}H_{11}^-$ anions. For further decomposition possibilities, we considered the dissociation energy of the CR radical and a BH fragment, which lead to breakdown and rearrangement of the cage. The results are presented in Figure 7.

The positive values for all energies suggest that every detachment process is endothermic, with considerably larger values for the CR radical and BH fragment detachments. Most of the fragments have similar energies between the two anions, with the notable exception that the energy to dissociate the CF radical is lower than the CH radical by approximately 2 eV. The energy for every process is slightly lower for the Mg^+ than the Mg^{2+} ion pairs, though still endothermic by our calculations. The chemical stability implied by these calculations and the similarity in bond dissociation energies for B−H bonds in $RCB_{11}H_{11}^-$ compared to those documented for the B−H bonds in BH_4^- indicates that each of these anions is stable with respect to Mg plating.[30,38]

Experimental determination of anion reductive stability is inferred from the Coulombic efficiency (CE, the ratio of charge recovered during stripping to that consumed during deposition) for Mg metal plating in a reductively stable solvent system. A direct comparison of the deposition and stripping response of the Mg salts of these anions in G3 (Mg^{2+} concentration ≈ 50 mM) is shown in Figure 8. $FCB_{11}H_{11}^-$ and $HCB_{11}H_{11}$ both yield 96% CE, an equivalency expected for two anions of nearly equivalent computed E_{red} (see Figure 4a). Noteworthy is the equivalency of the Mg nucleation

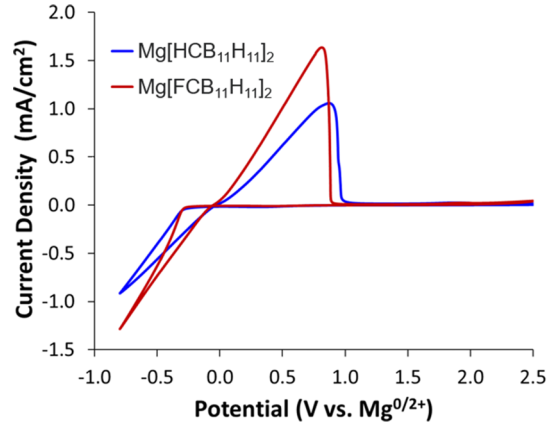

Figure 8. Voltammetric response of 50 mM $Mg[HCB_{11}H_{11}]_2$ and 50 mM $Mg[FCB_{11}H_{11}]_2$ in G3 (scan rate = 25 mV/s).

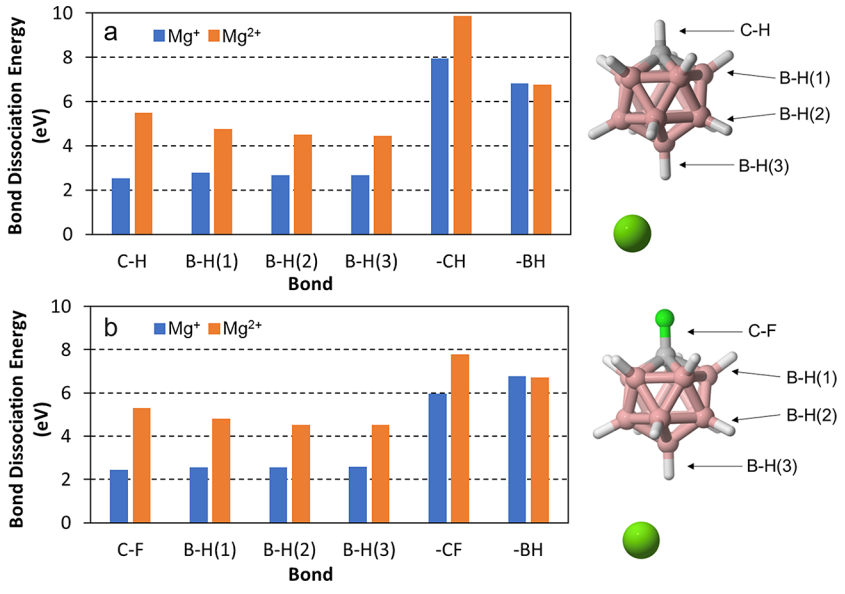

Figure 7. Bond/fragment dissociation energies for (a) $HCB_{11}H_{11}^-$ and (b) $FCB_{11}H_{11}^-$ when ion paired with Mg^{2+} or Mg^+.

DOI: 10.1021/jacs.8b05967
J. Am. Chem. Soc. 2018, 140, 11076−11084

overpotential of 290 mV onto Pt arguing these anions contribute equally to the energetic barrier for first deposition. The measured 4% inefficiency due to parasitic reactions over the −290 to −800 mV potential region is likely due to reductively unstable impurities within G3. The fraction of charge consumed by parasitic reduction during voltammetry is expected to scale inversely with the $Mg[RCB_{11}H_{11}]_2$ concentration. We qualitatively observe this expected relationship with an increase in CE to >99% for an approximate 5-fold increase in concentration to 250 mM $Mg[HCB_{11}H_{11}]_2$ in G3. Low concentrations were used in this comparative study due to the low quantity of available $FCB_{11}H_{11}^-$ salt after purification. Whereas the less stable $TFSI^-$ anion is found to passivate the Mg surface,[39,40] the parent and the derivative $RCB_{11}H_{11}^-$ anions do not impede dissolution of Mg during voltammetry, demonstrating that anion decomposition at the Mg surface is not operative for either anion. The presented computational and experimental data corroborates the chemical stability observed for $HCB_{11}H_{11}^-$ during cycling and shows a comparably stable configuration for the derivative anion, $FCB_{11}H_{11}^-$.

CONCLUSIONS

In this paper, we demonstrate that derivatization can be used to knowledgeably guide the enhancement of an anion's electrochemical stability. We show that the anodic stability of the $HCB_{11}H_{11}^-$ anion is defined by its oxidation to a neutral radical at 4.6 V (vs $Mg^{0/2+}$) independent of the solvent employed. This lower than projected value defines $HCB_{11}H_{11}^-$ with an anodic stability below that of conventional WCAs, including $TFSI^-$ and BF_4^-. The stability of $HCB_{11}H_{11}^-$ can be increased through fluorination of the carbon vertex, as revealed through high-throughput, first-principles computational screening and validated experimentally. We demonstrate the E_{ox} of $FCB_{11}H_{11}^-$ is increased by 300 mV without loss in cathodic stability when plating and stripping Mg in triglyme, as predicted through computed endothermic bond dissociation energies for the parent and fluorinated anion. Decreased calculated Mg^{2+}−anion binding strength argues for improved conductivity, as experimentally validated, and charge transfer for the fluorinated anion. The instability of oxidatively produced $RCB_{11}H_{11}^{\bullet}$ radicals in either the H- or F-terminated anion cases leads to rapid reaction with the anion, solvent, or impurities resulting in passivating film formation, limiting the extent of further electrolyte oxidation. This limiting behavior could represent a unique intrinsic electrolyte protection scheme for the carba-*closo*-borate class, provided these films conduct Mg^{2+} with suitable mobility. We believe that uncovering the origin of performance of these electrolytes at the molecular level grants insight that can be used toward future rational electrolyte design.

EXPERIMENTAL SECTION

Reagents. All carba-*closo*-dodecaborate salts were generated from either trimethylammonium ($TMAH^+$) or cesium $HCB_{11}H_{11}^-$ precursors purchased from Katchem, Ltd. and used as received. Triethylammonium chloride (TEAHCl, Sigma-Aldrich), butyl-methyl-pyrrolidinium chloride ($Py_{14}Cl$, Io-li-tec), and tetrabutylammonium hydroxide (TBAOH, 1 M in methanol, Sigma-Aldrich) were used as received. Tetrabutylammonium (TBA) salts of $TFSI^-$ and BF_4^- (99% purity) were purchased from Sigma-Aldrich and Fluka, respectively, and dried as needed to yield a total solution water content < 15 ppm. Ferrocene (Fc, 98%) was purchased from Sigma-Aldrich and used as received. Tetrahydrofuran (THF, 99.9%), acetonitrile (MeCN, 99.93%), and 1,1,1,3,3,3-hexafluoro-2-propanol (HFIP, 99%) were purchased in anhydrous form from Sigma-Aldrich. 1,2-Dimethoxyethane (DME), triethylene glycol dimethyl ether (G3), and tetraethylene glycol dimethyl ether (G4) were purchased from Sigma-Aldrich, treated with activated alumina, and distilled prior to use. 3-Methylsulfolane (3-MeTMS, 98%) was purchased from TCI. All solvents were stored over 3A and 4A molecular sieves and yielded water content < 10 ppm. *N*-Fluorobis(benzenesulfonyl)imide (NFSI), *n*-butyllithium solution (1.6 M in hexanes), and di-*n*-butylmagnesium solution (1 M in heptane) were purchased from Sigma-Aldrich and used as received.

Synthesis. Synthesis of $TBA[HCB_{11}H_{11}]$ was accomplished by reaction of $TMAH[HCB_{11}H_{11}]$ with TBAOH (25% excess) in a water/methanol solution. The resulting white powder was washed with excess water to remove residual TBAOH and recrystallized from water/isopropanol/acetone to yield a fine, white powder. ^1H NMR confirmed complete elimination of both $TMAH^+$ and OH^- from the resulting product. C fluorination of $HCB_{11}H_{11}^-$ was accomplished using established synthetic methods.[41] Similar to reported results, the as-synthesized product ($TEAH^+$ salt) contained 70−80% of the desired $FCB_{11}H_{11}^-$ species (with 20−30% unreacted $HCB_{11}H_{11}^-$) as determined by ^{11}B NMR. Purity was increased by multiple recrystallizations from acetone/water to 85−90% $FCB_{11}H_{11}^-$ based on ^{11}B NMR analysis (Supporting Information, Figure S7). $FCB_{11}H_{11}^-$ purity was further increased to 99.8% through HPLC.[41] Syntheses of $Mg[FCB_{11}H_{11}]_2$ and $Mg[HCB_{11}H_{11}]_2$ were accomplished by reaction of the corresponding $TEAH^+$ or $TMAH^+$ salt either with Mg shavings in G3 (for Mg plating experiments in G3) or with di-*n*-butylmagnesium in THF to produce dry salt for subsequent anodic characterization in 3-MeTMS. In the latter case, synthesis of the insoluble $Mg[RCB_{11}H_{11}]_2$ salt in THF was followed by filtration and drying under vacuum to produce a white powder containing THF of solvation (Supporting Information, Figure S8). Dissolution of this salt in 3-MeTMS followed by heating to 90 °C for a few hours was sufficient to remove the THF, based on ^1H NMR analysis.

Characterization. Nuclear magnetic resonance (NMR) characterization of the $RCB_{11}H_{11}^-$ salts was accomplished using a Bruker AVANCE 500 MHz instrument using standard borosilicate sample tubes. The broad ^{11}B signature from the borosilicate glass was subtracted from the spectra across the region of interest. X-ray photoelectron spectroscopy (XPS) was performed on a Kratos Supra spectrometer using a monochromatic Al Kα source and charge compensation. The binding energy axis was calibrated within each data set by defining the adventitious C 1s component binding energy as 284.8 eV. Time-of-flight secondary ion mass spectrometry (ToF-SIMS) was performed on an IONTOF TOF.SIMS 5 spectrometer with the liquid metal source tuned for the Bi_5^+ cluster.

Electrochemical behavior was characterized in BASi Inc. beaker-style cells with polished disk working electrodes (Pt−0.02 cm^2 and glassy carbon −0.071 cm^2) set within CTFE sleeves. Unless otherwise specified, reported electrochemical behavior is for Pt electrodes. Reference electrodes consisted of a Ag wire immersed in a 0.25 M $AgBF_4$ solution (either 3-MeTMS or MeCN as the supporting solvent) and separated from the bulk electrolyte by a Vycor frit. This reference electrode was calibrated in each electrolyte system of interest using the reversible half-wave potential of the ferrocene/ferrocenium ($Fc^{0/+}$) couple, which was determined to be +2.6 V vs $Mg^{0/2+}$ based on calibration in solutions yielding reversible Mg deposition (Supporting Information, Figure S9). The potentials of the Ag/Ag^+ reference electrodes were found to lie at +2.6 V vs $Mg^{0/2+}$ (MeCN) and +2.8 V vs $Mg^{0/2+}$ (3-MeTMS). Data is displayed with respect to $Mg^{0/2+}$, while comparative discussion is referenced to $Fc^{0/+}$. Fc-based redox probe passivation experiments were carried out using a Fc concentration of ∼13 mM in an electrolyte having the same solvent and salt composition as the electrolyte in which electrode polarization was performed. The working electrode was thoroughly rinsed and dried when transferred between electrolytes. Electrochemical measurements where made using a Solartron Modulab XM potentiostat with a frequency response analyzer. Conductivity was measured using a 1.14 cm^{-1} Pt cell calibrated with 1−100 mM

DOI: 10.1021/jacs.8b05967
J. Am. Chem. Soc. 2018, 140, 11076−11084

KCl(aq) solutions. Electrodes for XPS and ToF-SIMS analysis were prepared using a custom PTFE cell designed to accommodate a planar, textured Pt film created by evaporating 200 nm Pt onto undoped Si coated with a 20 nm Ti adhesion layer. Prior to electrochemical treatment the Pt surface was cleaned with acetone followed by H_2O_2/H_2SO_4 1:3 (piranha solution), thoroughly rinsed with deionized water, and vacuum dried.

Computational Methods. Derivations of the original $HCB_{11}H_{11}^-$ anion were explored by computational screening for (i) anodic stability (ionization potential), (ii) reductive stability (electron affinity), and (iii) ion-paired Mg^+ stability. Calculations were carried out using Gaussian 09[42] with an ultrafine integration grid at the B3LYP-D3(BJ)/6-311++G(d,p)//B3LYP/6-31+g(d) level of theory.[43−46] Solvent effects were accounted for with the PCM method[47,48] in the single-point energy calculations on the gas-phase-optimized structures using triglyme as the solvent. To model anodic and cathodic stabilities, ionization potentials (IPs) and electron affinities (EAs) were computed under the adiabatic approximation,[49,50] which accounts for orbital and geometric relaxation between charge states. These computed values are converted to oxidation and reduction potentials, respectively, referenced to Mg by assuming the $Mg^{0/2+}$ standard reduction potential at −2.37 V vs SHE corresponds to an absolute electrode potential of 2.06 eV relative to the vacuum level. Vibrational frequencies were computed to ensure the absence of imaginary frequencies and that all geometries are minima on the potential energy surface. Molecular graphics were generated with CYLview.[51]

■ ASSOCIATED CONTENT

Supporting Information

The Supporting Information is available free of charge on the ACS Publications website at DOI: 10.1021/jacs.8b05967.

Voltammetric demonstration of glyme oxidation thresholds; voltammetric demonstration of cation and electrode independent oxidation of $HCB_{11}H_{11}^-$ anion; ToF-SIMS results demonstrating the dominance of the carborate cage in passive films formed through $HCB_{11}H_{11}^-$ anion oxidation; voltammetric results of a low concentration $HCB_{11}H_{11}^-$ anion at a high potential sweep rate in MeCN; voltammetric results of $HCB_{11}H_{11}^-$ anion at slow potential sweep rate in MeCN; computed electrochemical oxidation and reduction potentials for all $RCB_{11}H_{11}^-$ anions considered in this study; binding strength of Mg^{2+}/ $RCB_{11}H_{11}^-$ (R = H, F) ion pairs with an explicitly modeled G3 solvent molecule; NMR results demonstrating the purity of synthesized $FCB_{11}H_{11}^-$ anion; NMR results demonstrating $Mg[HCB_{11}H_{11}]_2$ and $Mg[FCB_{11}H_{11}]_2$ synthesis; graphic explanation of reference electrode calibration (PDF)

■ AUTHOR INFORMATION

Corresponding Authors

*krzavad@sandia.gov

*kapersson@lbl.gov

ORCID

Nathan T. Hahn: 0000-0001-6187-4068

Ka-Cheong Lau: 0000-0002-3726-163X

Chen Liao: 0000-0001-5168-6493

Kristin A. Persson: 0000-0003-2495-5509

Kevin R. Zavadil: 0000-0002-3791-424X

Author Contributions

‖N.T.H. and T.J.S.: These authors contributed equally.

Notes

The authors declare no competing financial interest.

■ ACKNOWLEDGMENTS

This work was supported as part of the Joint Center for Energy Storage Research, an Energy Innovation Hub funded by the U.S. Department of Energy, Office of Science, Basic Energy Sciences. This research used the Savio computational cluster resource provided by the Berkeley Research Computing program at the University of California, Berkeley. Sandia National Laboratories, is a multimission laboratory managed and operated by National Technology and Engineering Solutions of Sandia, LLC., a wholly owned subsidiary of Honeywell International, Inc., for the U.S. Department of Energy's National Nuclear Security Administration under contract DE-NA-0003525.

■ REFERENCES

(1) Xu, K. *Chem. Rev.* **2014**, *114* (23), 11503−11618.

(2) Tutusaus, O.; Mohtadi, R.; Arthur, T. S.; Mizuno, F.; Nelson, E. G.; Sevryugina, Y. V. *Angew. Chem., Int. Ed.* **2015**, *54* (27), 7900−7904.

(3) Zhao-Karger, Z.; Gil Bardaji, M. E.; Fuhr, O.; Fichtner, M. *J. Mater. Chem. A* **2017**, *5* (22), 10815−10820.

(4) Herb, J. T.; Nist-Lund, C. A.; Arnold, C. B. *Acs Energy Lett.* **2016**, *1* (6), 1227−1232.

(5) Yoo, H. D.; Shterenberg, I.; Gofer, Y.; Gershinsky, G.; Pour, N.; Aurbach, D. *Energy Environ. Sci.* **2013**, *6* (8), 2265−2279.

(6) Muldoon, J.; Bucur, C. B.; Gregory, T. *Angew. Chem., Int. Ed.* **2017**, *56* (40), 12064−12084.

(7) Aurbach, D.; Lu, Z.; Schechter, A.; Gofer, Y.; Gizbar, H.; Turgeman, R.; Cohen, R.; Moshkovich, M.; Levi, E. *Nature* **2000**, *407*, 724−727.

(8) Pour, N.; Gofer, Y.; Major, D. T.; Aurbach, D. *J. Am. Chem. Soc.* **2011**, *133* (16), 6270−6278.

(9) Liu, T. B.; Shao, Y. Y.; Li, G. S.; Gu, M.; Hu, J. Z.; Xu, S. C.; Nie, Z. M.; Chen, X. L.; Wang, C. M.; Liu, J. *J. Mater. Chem. A* **2014**, *2* (10), 3430−3438.

(10) Chen, T. N.; Sai Gautam, G.; Huang, W. X.; Ceder, G. *Chem. Mater.* **2018**, *30* (1), 153−162.

(11) Keyzer, E. N.; Glass, H. F. J.; Liu, Z.; Bayley, P. M.; Dutton, S. E.; Grey, C. P.; Wright, D. S. *J. Am. Chem. Soc.* **2016**, *138*, 8682−8685.

(12) Shterenberg, I.; Salama, M.; Gofer, Y.; Aurbach, D. *Langmuir* **2017**, *33* (37), 9472−9478.

(13) McArthur, S. G.; Geng, L. X.; Guo, J. C.; Lavallo, V. *Inorg. Chem. Front.* **2015**, *2* (12), 1101−1104.

(14) Carter, T. J.; Mohtadi, R.; Arthur, T. S.; Mizuno, F.; Zhang, R. G.; Shirai, S.; Kampf, J. W. *Angew. Chem., Int. Ed.* **2014**, *53* (12), 3173−3177.

(15) McArthur, S. G.; Jay, R.; Geng, L. X.; Guo, J. C.; Lavallo, V. *Chem. Commun.* **2017**, *53* (32), 4453−4456.

(16) Wiersema, R. J.; Hawthorne, M. F. *Inorg. Chem.* **1973**, *12* (4), 785−788.

(17) Boere, R. T.; Bolli, C.; Finze, M.; Himmelspach, A.; Knapp, C.; Roemmele, T. L. *Chem. - Eur. J.* **2013**, *19* (5), 1784−1795.

(18) Wahab, A.; Douvris, C.; Klima, J.; Sembera, F.; Ugolotti, J.; Kaleta, J.; Ludvik, J.; Michl, J. *Inorg. Chem.* **2017**, *56* (1), 269−276.

(19) Fleischmann, M.; Pletcher, D. *Tetrahedron Lett.* **1968**, *9*, 6255−6258.

(20) Portis, L. C.; Mann, C. K.; Roberson, J. C. *Anal. Chem.* **1972**, *44* (2), 294−297.

(21) Cassidy, J.; Khoo, S. B.; Pons, S.; Fleischmann, M. *J. Phys. Chem.* **1985**, *89* (18), 3933−3935.

(22) Borodin, O.; Ren, X. M.; Vatamanu, J.; von Wald Cresce, A.; Knap, J.; Xu, K. *Acc. Chem. Res.* **2017**, *50* (12), 2886−2894.

DOI: 10.1021/jacs.8b05967
J. Am. Chem. Soc. 2018, 140, 11076−11084

(23) Kim, D. Y.; Park, M. S.; Lim, Y.; Kang, Y. S.; Park, J. H.; Doo, S. G. *J. Power Sources* **2015**, *288*, 393−400.
(24) Francke, R.; Cericola, D.; Kotz, R.; Weingarth, D.; Waldvogel, S. R. *Electrochim. Acta* **2012**, *62*, 372−380.
(25) Tourillon, G.; Lacaze, P. C.; Dubois, J. E. *J. Electroanal. Chem. Interfacial Electrochem.* **1979**, *100* (1−2), 247−262.
(26) Cheng, L.; Assary, R. S.; Qu, X. H.; Jain, A.; Ong, S. P.; Rajput, N. N.; Persson, K.; Curtiss, L. A. *J. Phys. Chem. Lett.* **2015**, *6* (2), 283−291.
(27) Johansson, P.; Jacobsson, P. *J. Power Sources* **2006**, *153* (2), 336−344.
(28) Lapidus, S. H.; Rajput, N. N.; Qu, X. H.; Chapman, K. W.; Persson, K. A.; Chupas, P. J. *Phys. Chem. Chem. Phys.* **2014**, *16* (40), 21941−21945.
(29) Qu, X. H.; Zhang, Y.; Rajput, N. N.; Jain, A.; Maginn, E.; Persson, K. A. *J. Phys. Chem. C* **2017**, *121* (30), 16126−16136.
(30) Rajput, N. N.; Qu, X. H.; Sa, N.; Burrell, A. K.; Persson, K. A. *J. Am. Chem. Soc.* **2015**, *137* (9), 3411−3420.
(31) Jelínek, T. B.; Baldwin, P.; Scheidt, W. R.; Reed, C. A. *Inorg. Chem.* **1993**, *32* (10), 1982−1990.
(32) Teruo, U.; Sumi, I. *Tetrahedron Lett.* **1990**, *31* (25), 3579−3582.
(33) Eisenberger, P.; Gischig, S.; Togni, A. *Chem. - Eur. J.* **2006**, *12* (9), 2579−2586.
(34) Wang, X.; Ye, X.; Zhang, S.; Feng, J.; Xu, Y.; Zhang, Y.; Wang, J. *J. Am. Chem. Soc.* **2011**, *133* (41), 16410−16413.
(35) Fujiwara, Y.; Dixon, J. A.; O'Hara, F.; Funder, E. D.; Dixon, D. D.; Rodriguez, R. A.; Baxter, R. D.; Herlé, B.; Sach, N.; Collins, M. R.; Ishihara, Y.; Baran, P. S. *Nature* **2012**, *492*, 95−99.
(36) Baskin, A.; Prendergast, D. *J. Phys. Chem. C* **2016**, *120* (7), 3583−3594.
(37) Crowther, D. J.; Borkowsky, S. L.; Swenson, D.; Meyer, T. Y.; Jordan, R. F. *Organometallics* **1993**, *12* (8), 2897−2903.
(38) Mohtadi, R.; Matsui, M.; Arthur, T. S.; Hwang, S. J. *Angew. Chem., Int. Ed.* **2012**, *51* (39), 9780−9783.
(39) Sa, N. Y.; Pan, B. F.; Saha-Shah, A.; Hubaud, A. A.; Vaughey, J. T.; Baker, L. A.; Liao, C.; Burrell, A. K. *ACS Appl. Mater. Interfaces* **2016**, *8* (25), 16002−16008.
(40) Shterenberg, I.; Salama, M.; Yoo, H. D.; Gofer, Y.; Park, J. B.; Sun, Y. K.; Aurbach, D. *J. Electrochem. Soc.* **2015**, *162* (13), A7118−A7128.
(41) Janousek, Z.; Hilton, C. L.; Schreiber, P. J.; Michl, J. *Collect. Czech. Chem. Commun.* **2002**, *67* (7), 1025−1034.
(42) Frisch, M. J.; Trucks, G. W.; Schlegel, H. B.; Scuseria, G. E.; Robb, M. A.; Cheeseman, J. R.; Scalmani, G.; Barone, V.; Mennucci, B.; Petersson, G. A.; Nakatsuji, H.; Caricato, M.; Li, X.; Hratchian, H. P.; Izmaylov, A. F.; Bloino, J.; Zheng, G.; Sonnenberg, J. L.; Hada, M.; Ehara, M.; Toyota, K.; Fukuda, R.; Hasegawa, J.; Ishida, M.; Nakajima, T.; Honda, Y.; Kitao, O.; Nakai, H.; Vreven, T.; Montgomery, J. A., Jr.; Peralta, J. E.; Ogliaro, F.; Bearpark, M.; Heyd, J. J.; Brothers, E.; Kudin, K. N.; Staroverov, V. N.; Kobayashi, R.; Normand, J.; Raghavachari, K.; Rendell, A.; Burant, J. C.; Iyengar, S. S.; Tomasi, J.; Cossi, M.; Rega, N.; Millam, N. J.; Klene, M.; Knox, J. E.; Cross, J. B.; Bakken, V.; Adamo, C.; Jaramillo, J.; Gomperts, R.; Stratmann, R. E.; Yazyev, O.; Austin, A. J.; Cammi, R.; Pomelli, C.; Ochterski, J. W.; Martin, R. L.; Morokuma, K.; Zakrzewski, V. G.; Voth, G. A.; Salvador, P.; Dannenberg, J. J.; Dapprich, S.; Daniels, A. D.; Farkas, Ö.; Foresman, J. B.; Ortiz, J. V.; Cioslowski, J.; Fox, D. J. *Gaussian 09*, Revision D.01; Gaussian, Inc.: Wallingford, CT, 2009.
(43) Becke, A. D. *J. Chem. Phys.* **1993**, *98* (7), 5648−5652.
(44) Grimme, S.; Antony, J.; Ehrlich, S.; Krieg, H. *J. Chem. Phys.* **2010**, *132* (15), 154104.
(45) Johnson, E. R.; Becke, A. D. *J. Chem. Phys.* **2006**, *124* (17), 174104.
(46) Stephens, P. J.; Devlin, F. J.; Chabalowski, C. F.; Frisch, M. J. *J. Phys. Chem.* **1994**, *98* (45), 11623−11627.
(47) Miertus, S.; Scrocco, E.; Tomasi, J. *Chem. Phys.* **1981**, *55* (1), 117−129.
(48) Tomasi, J.; Mennucci, B.; Cammi, R. *Chem. Rev.* **2005**, *105* (8), 2999−3093.
(49) Ong, S. P.; Ceder, G. *Electrochim. Acta* **2010**, *55* (11), 3804−3811.
(50) Qu, X. H.; Jain, A.; Rajput, N. N.; Cheng, L.; Zhang, Y.; Ong, S. P.; Brafman, M.; Maginn, E.; Curtiss, L. A.; Persson, K. A. *Comput. Mater. Sci.* **2015**, *103*, 56−67.
(51) Legault, C. Y. *CYLview 1.0b*; Université de Sherbrooke, 2009.

DOI: 10.1021/jacs.8b05967
J. Am. Chem. Soc. 2018, 140, 11076−11084